Indian Journal of Pure & Applied Physics
Vol. 52, October 2014, pp. 653-670

Vibrational and quantum chemical analysis of 3-methyl-2,6-diphenyl piperidin-4-one using HF and DFT methods

A Thirunavukkarasu[1], R Karunathan[2], J Mallika[3] & V Sathyanarayanamoorthi[2]*

[1]Department of Physics, K S Rangasamy College of Technology, Tiruchengode, Namakkal 637 215 Tamil Nadu, India

[2]Department of Physics, P S G College of Arts & Science, Coimbatore 641 014, Tamil Nadu, India

[3]Department of Chemistry, P S G College of Arts & Science, Coimbatore 641 014, Tamil Nadu, India

*E-mail: sathyanarayanamoorthi@yahoo.co.in

Received 11 June 2013; revised 16 December 2013; accepted 3 April 2014

Characterization of 3-methyl-2,6-diphenylpiperidin-4-one (MDPO) by quantum chemical calculations and spectral techniques has been performed with spectroscopic investigations like FT-IR, FT-Raman and UV techniques. Molecular geometries, FT-IR spectrum (4000-400 cm^{-1}) and FT-Raman spectrum (4000-100 cm^{-1}) in solid phase was recorded. The structural and spectroscopic data of the molecule were obtained from HF and B3LYP with 6-311++G(d,p) levels using density functional theory(DFT). The stability and intra-molecular charge transfer have been analyzed by the detailed natural bond orbital (NBO) analysis. The charge transfer occurring in the molecule was verified and found to be stable from smaller energy gap by HOMO-LUMO analysis. Atomic population analysis reveals the percentage of electron distribution in s-and p-subshells. The first order hyperpolarizability of the investigated molecule has been studied theoretically. The calculated results were applied to simulated infrared and Raman spectra of the title molecule which show good agreement with observed spectra.

Keywords: DFT, HOMO, LUMO, Natural Bond Orbital, Hyperpolarizability, UV spectra

1 Introduction

Piperidine derivatives were found to possess pharmacological activity. They are the essential part of molecular structures in important drugs[1]. Piperidone derivatives as prospective biophotonic materials has been explored recently. Piperidines form an important framework and served as precursors for chiral biologically active natural alkaloids. Their biological activity is excellent if 2-and/or 6-positions are occupied by aryl groups. Its anti-bacterial and anti-fungal activities have been explored well. 2,6-diaryl piperidine4-one have been subjected to quite a large number of synthetic and physico-chemical studies.Piperidine-4-one pharmacophore is present in a wide variety of naturally occurring alkaloids and is responsible for a number of biological actions such as anti-bacterial, anti-fungal, anti-tuberchlostic, anti-cancer,anti-oxidant, anti-inflammatory neuronal nicotinic antagonistic activity, CNS stimulant, depressant[2-6]. Miglitol, a piperidine derivative, is primarily used in diabetes mellitus type-2 for establishing greater glycemic control by preventing the digestion of carbohydrates into monosaccharides which can be absorbed by body[7]. Piperidine is used as a rubber vulcanization accelerator. In pharmaceutical synthesis industry, it is a special solvent and as a protecting group for peptide synthesis. Piperidine derivative compounds are used as intermediate to make crystal derivative of aromatic nitrogen compounds containing nuclear halogen atoms. It is a structural element for pharma drugs like raloxifene and minoxidil. Ring system compounds with nitrogen which have basic properties play important role as cyclic compounds in the industrial field such as raw materials for hardness of epoxy resins, corrosion inhibitors, insecticides, accelerators for rubber, urethane catalysts, anti-oxidants and as a catalyst for silicone esters[8]. The theoretical *ab-initio*, DFT, and spectroscopical analysis of the title molecule give information regarding the nature of the electronic structure, the functional groups and orbital interactions and mixing of vibrational frequencies[36-38].

2 Experimental Details

2.1 Synthesis of MDPO

To a solution of dry ammonium acetate (9.8 g, 0.125 mol) in glacial acetic acid (12.5 g, 0.21 mol) was added benzaldehyde (29 g, 0.25 mol) and butanone (9 g, 0.125 mol). The mixture was just heated to boil and allowed to stand overnight at room temperature. The concentrated hydrochloric acid (13 ml) was added, the precipitated hydrochloride was collected and washed with ethanol-ether (1:5) mixture. Crystallization from ethanol-ether yielded the pure hydrochloride, mp (223-225°C) (lit 224-226°C)

A suspension of the hydrochloride in acetone was treated with ammonia (1:1) and the free base was obtained by diluting with large amount of water. Crystallization of the product from ethanol[39,40] gave 3-methyl-2,6-diphenylpiperidin-4-one mp(96-97°C) (lit 96-97°C).

2.2 FT-Raman and FT-IR measurement

FT-Raman spectrum of MDPO was recorded using ND: YAG laser as excitation wavelength in the region 50-4000 cm^{-1} using BRUKER RFS 27 standalone spectrometer. The ND:YAG laser source operates at 1064nm line with 200 mW powers. The FT-IR spectrum of the MDPO was recorded using PERKIN-ELMER spectrometer in the region 4000-100 cm^{-1}. The frequencies of all sharp bands are accurate to ± 1 cm^{-1}.

3 Computational Details

The molecular geometry optimization and vibrational frequency calculations were carried out for MDPO using GAUSSIAN 09 software[9]. HFfunctional[10,11] combined with standard basis set HF/6-311++G(d,p) and denstity functional method B3LYP/6-31++G(d,p) used is B3LYP i.e., Becke's three-parameter hybrid functional with Lee-Yang-Parr correlation method[12,13]. The Raman activities (S^A) calculated with Gaussian 09 program were converted to relative Raman intensities (I^{RA}) using the following relationship derived from the intensity theory of Raman scattering[14,15].

$$I_{RA} = \frac{f(\upsilon_o - \upsilon_i)^4 S_i}{\upsilon_i[1-\exp(-hc\upsilon_i / kt)]}$$

where υ_o is the exciting frequency in cm^{-1}, υ_i the vibrational wavenumber of the (i^{th}) normal mode, *h, c* and *k* are fundamental constants.

4 Results and Discussion

4.1 Moecular Geometry

The bond lengths and bond angles of MDPO are given in Table 1. The optimized structure of MDPO

Table 1 — Bond lengths. bond angles, torsional angles and dihedral angles of MDPO

Bond length (Å)	HF 6-311++G(d,p)	B3LYP 6-311++G(d,p)
N_1— C_2	1.4696	1.4863
N_1—C_6	1.4551	1.4749
N_1—H_{21}	0.9977	1.0118
C_2—C_3	1.5500	1.5662
C_2—C_{15}	1.5240	1.5256
C_2— H_{22}	1.0859	1.0954
C_3—C_4	1.5206	1.5215
C_3—C_8	1.5247	1.5302
C_3—H_{23}	1.0900	1.0993
C_4—C_5	1.5171	1.5156
C_4—O_7	1.1881	1.2409
C_5—C_6	1.5308	1.5411
C_5— H_{24}	1.0843	1.0927
C_5—H_{25}	1.0864	1.0945
C_6—C_9	1.5189	1.5216
C_6—H_{26}	1.0912	1.1031
C_8—H_{27}	1.0829	1.0893
C_8—H_{28}	1.0851	1.0915
C_8—H_{29}	1.0840	1.0902
C_9—C_{10}	1.3875	1.4018
C_9—C_{14}	1.3922	1.4039
C_{10}—C_{11}	1.3877	1.3985
C_{10}—H_{30}	1.0766	1.0840
C_{11}—C_{12}	1.3828	1.3971
C_{11}—H_{31}	1.0756	1.0824
C_{12}—C_{13}	1.3873	1.3991
C_{12}—H_{32}	1.0754	1.0822
C_{13}—C_{14}	1.3836	1.3968
C_{13}—H_{33}	1.0757	1.0825
C_{14}—H_{34}	1.0745	1.0817
C_{15}—C_{16}	1.3869	1.4015
C_{15}—C_{20}	1.3935	1.4051
C_{16}—C_{17}	1.3886	1.3990
C_{16}—C_{35}	1.0761	1.0834
C_{17}—C_{18}	1.3820	1.3965
C_{17}—H_{36}	1.0756	1.0824
C_{18}—C_{19}	1.3879	1.3997
C_{18}—H_{37}	1.0753	1.0821
C_{19}—C_{20}	1.3826	1.3962
C_{19}—H_{38}	1.0757	1.0825
C_{20}—H_{39}	1.0757	1.0832
Bond angle (degrees)		
C_2—N_1—C_6	118.1421	119.5862
C_2—N_1—H_{21}	110.7908	112.8618
C_6—N_1—H_{21}	111.2114	113.3203
N_1—C_2—C_3	111.7473	110.8473
N_1—C_2—C_{15}	112.3014	112.0902
N_1—C_2— H_{22}	107.1556	108.1676
C_3—C_2— C_{15}	112.1656	111.9976
C_3—C_2—H_{22}	106.3564	106.1665
C_{15}—C_2—H_{22}	106.6641	107.2517
C_2— C_3—C_4	109.4959	109.5225
C_2— C_3—C_8	112.8051	112.5910
C_2—C_3—H_{23}	107.9987	107.0186

Contd—

Table 1 — Bond lengths. bond angles, torsional angles and dihedral angles of MDPO — *Contd*

Bond length (Å)	HF 6-311++G(d,p)	B3LYP 6-311++G(d,p)
$C_4-C_3-C_8$	112.3059	112.6547
$C_4-C_3-H_{23}$	105.0768	105.7638
$C_8-C_3-H_{23}$	108.7786	108.9064
$C_3-C_4-C_5$	115.6936	116.5321
$C_3-C_4-O_7$	122.9754	122.3938
$C_5-C_4-O_7$	121.3272	121.0714
$C_4-C_5-C_6$	112.1782	112.5808
$C_4-C_5-H_{24}$	107.2525	107.8247
$C_4-C_5-H_{25}$	108.1954	108.7911
$C_6-C_5-H_{24}$	110.4382	109.8381
$C_6-C_5-H_{25}$	111.3081	110.9411
$H_{24}-C_5-H_{25}$	107.2536	106.6426
$N_1-C_6-C_5$	107.5251	107.4809
$N_1-C_6-C_9$	110.5987	110.4269
$N_1-C_6-H_{26}$	112.0906	112.0933
$C_5-C_6-C_9$	111.8117	111.9792
$C_5-C_6-H_{26}$	108.2941	108.0919
$C_9-C_6-H_{26}$	106.5525	106.8026
$C_3-C_8-H_{27}$	110.3982	110.5885
$C_3-C_8-H_{28}$	110.9205	110.8816
$C_3-C_8-H_{29}$	110.7194	110.7238
$H_{27}-C_8-H_{28}$	107.4610	107.1649
$H_{27}-C_8-H_{29}$	108.6149	108.7638
$H_{28}-C_8-H_{29}$	108.6294	108.6131
$C_6-C_9-C_{10}$	120.1457	120.3219
$C_6-C_9-C_{14}$	121.2441	120.8708
$C_{10}-C_9-C_{14}$	118.5987	118.7933
$C_9-C_{10}-C_{11}$	120.9245	120.7747
$C_9-C_{10}-H_{30}$	119.7477	119.5087
$C_{11}-C_{10}-H_{30}$	119.3277	119.7166
$C_{10}-C_{11}-C_{12}$	120.0437	120.0256
$C_{10}-C_{11}-H_{31}$	119.7670	119.8408
$C_{12}-C_{11}-H_{31}$	120.1887	120.1331
$C_{11}-C_{12}-C_{13}$	119.4906	119.6218
$C_{11}-C_{12}-H_{32}$	120.2803	120.1866
$C_{13}-C_{12}-H_{32}$	120.2288	120.1913
$C_{12}-C_{13}-C_{14}$	120.3572	120.2687
$C_{12}-C_{13}-H_{33}$	119.9699	119.9814
$C_{14}-C_{13}-H_{33}$	119.6729	119.7499
$C_9-C_{14}-C_{13}$	120.5842	120.5142
$C_9-C_{14}-H_{34}$	119.5295	119.1567
$C_{13}-C_{14}-H_{34}$	119.8850	120.3260
$C_2-C_{15}-C_{16}$	120.1095	120.2873
$C_2-C_{15}-C_{20}$	121.6304	121.2057
$C_{16}-C_{15}-C_{20}$	118.2531	118.5039
$C_{15}-C_{16}-C_{17}$	121.0493	120.9143
$C_{15}-C_{16}-H_{35}$	119.5844	119.3250
$C_{17}-C_{16}-H_{35}$	119.3663	119.7605
$C_{16}-C_{17}-C_{18}$	120.1219	120.0474
$C_{16}-C_{17}-H_{36}$	119.7164	119.8364
$C_{18}-C_{17}-H_{36}$	120.1614	120.1157
$C_{17}-C_{18}-C_{19}$	119.4225	119.6035
$C_{17}-C_{18}-H_{37}$	120.3551	120.2498
$C_{19}-C_{18}-H_{37}$	120.2221	120.1461
$C_{18}-C_{19}-C_{20}$	120.2364	120.1568

Contd—

Table 1 — Bond lengths. bond angles, torsional angles and dihedral angles of MDPO — *Contd*

Bond length (Å)	HF 6-311++G(d,p)	B3LYP 6-311++G(d,p)
$C_{18}-C_{19}-H_{38}$	120.0133	120.0040
$C_{20}-C_{19}-H_{38}$	119.7503	119.8392
$C_{15}-C_{20}-C_{19}$	120.9152	120.7720
$C_{15}-C_{20}-H_{39}$	120.1144	119.7788
$C_{19}-C_{20}-H_{39}$	118.9702	119.4481
Torsion angles (degrees)		
$C_5-C_6-C_9-C_{14}$	74.6653	73.8556
$C_5-C_6-C_9-C_{10}$	−104.0817	−104.7629
$C_3-C_2-C_{15}-C_{20}$	66.7939	69.6542
$C_3-C_2-C_{15}-C_{16}$	−114.1878	−111.005
$C_2-N_1-C_6-C_9$	−176.3563	179.8656
$C_6-N_1-C_2-C_{15}$	111.1078	114.8109
$C_4-C_5-C_6-N_1$	−46.7674	−46.8936
$C_1-C_2-C_3-C_4$	−39.9585	−42.5899
$C_6-C_9-C_{14}-C_{13}$	−178.5754	−178.3154
$C_6-C_9-C_{14}-C_{34}$	1.8512	2.3174
$C_2-C_{15}-C_{16}-C_{17}$	−179.5186	−179.8502
$C_2-C_{15}-C_{16}-C_{35}$	0.4216	−0.0212
$C_6-C_9-C_{10}-H_{30}$	−1.6909	−1.9074
$C_2-C_{15}-C_{20}-H_{39}$	−0.4061	0.2254
$C_2-C_{15}-C_{20}-C_{19}$	179.4228	179.8334
$N_1-C_6-C_9-C_{10}$	136.1223	135.5026
$C_6-C_9-C_{10}-C_{11}$	178.3901	178.1592
$N_1-C_2-C_3-C_8$	−165.8068	−168.7582
$C_2-N_1-C_6-C_9$	−176.3563	179.8656
Dihedral angles(degrees)		
$C_8-C_3-C_4-C_5$	177.9677	177.4545
$C_3-C_4-C_5-H_{24}$	−128.875	−126.4792
$N_1-C_6-C_9-C_{14}$	−45.1307	−45.8789
$C_2-C_3-C_4-O_7$	−128.8635	−129.2648
$O_7-C_4-C_5-C_6$	173.2403	175.4179
$H_{26}-C_6-C_9-C_{10}$	14.0606	13.3812
$H_{26}-C_6-C_9-C_{14}$	−167.1925	−168.0003
$BD^*(1)C_3-C_4$	0.05258	0.63425
$BD^*(1)C_3-C_8$	0.01009	0.61706
$BD^*(1)C_3-H_{23}$	0.01701	0.58065
$BD^*(1)C_4-C_5$	0.04249	0.62741
$BD^*(1)C_4-O_7$	0.01229	0.86930
$BD^*(2)C_4-O_7$	0.05680	0.20764
$BD^*(1)C_5-C_6$	0.02336	0.61113
$BD^*(1)C_5-H_{24}$	0.00906	0.60746
$BD^*(1)C_5-H_{25}$	0.01174	0.58040
$BD^*(1)C_6-C_9$	0.02540	0.68980
$BD^*(1)C_6-H_{26}$	0.05674	0.62151
$BD^*(1)C_8-H_{27}$	0.00461	0.60894
$BD^*(1)C_8-H_{28}$	0.00616	0.60021
$BD^*(1)C_8-H_{29}$	0.00473	0.59746
$BD^*(1)C_9-C_{10}$	0.02106	0.79621
$BD^*(2)C_9-C_{10}$	0.33779	0.16583
$BD^*(1)C_9-C_{14}$	0.02327	0.79137
$BD^*(1)C_{10}-C_{11}$	0.01238	0.78681
$BD^*(1)C_{10}-H_{30}$	0.01094	0.64409

Contd—

Table 1 — Bond lengths. bond angles, torsional angles and dihedral angles of MDPO — *Contd*

Bond length(Å)	HF 6-311++G(d,p)	B3LYP 6-311++G(d,p)
$BD^{*}(1)C_{11}–C_{12}$	0.01348	0.78862
$BD^{*}(2)C_{11}–C_{12}$	0.32724	0.15654
$BD^{*}(1)C_{11}–H_{31}$	0.01031	0.64911
$BD^{*}(1)C_{12}–C_{13}$	0.01351	0.78919
$BD^{*}(1)C_{12}–H_{32}$	0.01057	0.65192
$BD^{*}(1)C_{13}–C_{14}$	0.01284	0.79277
$BD^{*}(2)C_{13}–C_{14}$	0.31295	0.16319
$BD^{*}(1)C_{13}–H_{33}$	0.01061	0.65130
$BD^{*}(1)C_{14}–H_{34}$	0.01048	0.66030
$BD^{*}(1)C_{15}–C_{16}$	0.02079	0.78368
$BD^{*}(2)C_{15}–C_{16}$	0.33061	0.15486
$BD^{*}(1)C_{15}–C_{20}$	0.02516	0.77248
$BD^{*}(1)C_{16}–C_{17}$	0.01252	0.77647
$BD^{*}(1)C_{16}–H_{35}$	0.01099	0.63166
$BD^{*}(1)C_{17}–C_{18}$	0.01329	0.77773
$BD^{*}(2)C_{17}–C_{18}$	0.32384	0.14697
$BD^{*}(1)C_{17}–H_{36}$	0.01027	0.64069
$BD^{*}(1)C_{18}–C_{19}$	0.01302	0.77600
$BD^{*}(1)C_{18}–H_{37}$	0.01040	0.64210
$BD^{*}(1)C_{19}–C_{20}$	0.01646	0.77983
$BD^{*}(2)C_{19}–C_{20}$	0.34482	0.14943
$BD^{*}(1)C_{19}–H_{38}$	0.01037	0.63444
$BD^{*}(1)C_{20}–H_{39}$	0.01749	0.63644

along with the atom numbering schemes is shown in Fig. 1. This compound has N–H bond, C–O bond, C–N bonds, C–H bonds and C–C bonds. $C_4–O_7$ average bond length 1.20Å. C–C bond length is usually observed[16] to be nearly equal to 1.400Å. In the present investigation, bond lengths of $C_2–C_3$, $C_2–C_{15}$, $C_3–C_4$, $C_3–C_8$, $C_4–C_5$, $C_5–C_6$, and $C_6–C_9$ are in line with 1.400Å values. Bond distances of $C_9–C_{10}$, $C_9–C_{14}$, $C_{10}–C_{11}$, $C_{11}–C_{12}$, $C_{12}–C_{13}$, $C_{13}–C_{14}$, $C_{15}–C_{16}$, $C_{15}–C_{20}$, $C_{16}–C_{17}$, $C_{17}–C_{18}$, $C_{18}–C_{19}$ are having a mean value of 1.39Å with few exceptions. Almost all C–H bond lengths calculated nearly equal to 1.00 Å. $N_1–H_{21}$ bond length is also nearly equal to 1.00 Å. Calculated values of $C_3–C_4–O_7$ and $C_5–C_4–O_7$ are 122.6° and 121.2°, respectively. These are larger bond angle which may be due to electron density in oxygen atoms. C–C–H bond angles are approximately equal to 120° (phenyl rings). Other than phenyl rings it is nearly equal to 109°. C–C–C angles vary from 109° to 120°. H–C–H and N–C–H angles are nearly equal to 108°. N–C–C angles calculated at both HF and B3LYP methods are nearly equal to 111°. The only $C_2–N_1–C_6$ bond angle is 118°. The dihedral angles

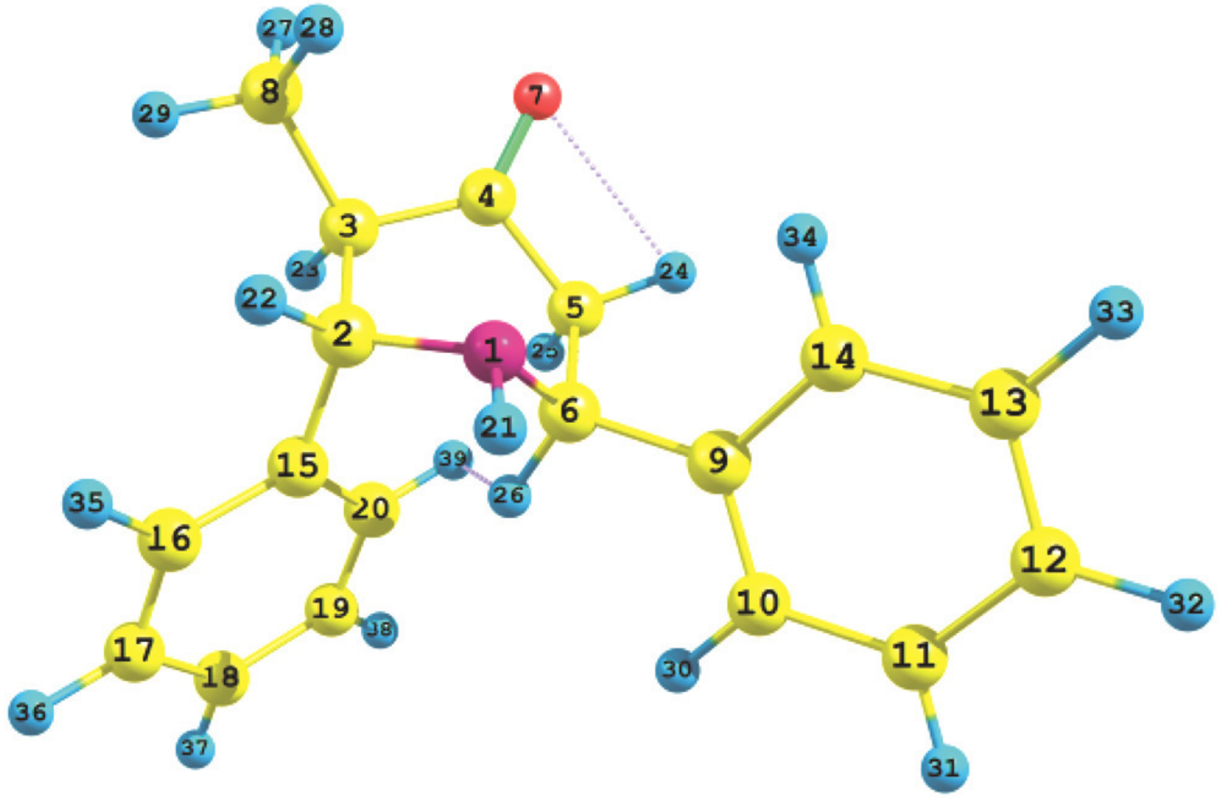

Fig. 1 — Optimized molecular structure of 3-methyl-2, 6-diphenylpiperidin-4-one(MDPO)

between piperidine and phenyl rings are given in Table 1. A few torsional angles of the title compound MDPO are also given in Table 1.

4.2 Vibrational assignments

The title molecule MDPO consists of 39 atoms and hence it has 111 normal modes of vibrations. According to classical mechanics, the molecule has 111 normal modes of vibration. For a proper understanding of the IR and Raman spectra of polyatomic molecules typically with modes of vibration exceeding beyond 50, DFT method gives the more accurate prediction other than calculation methods[36]. The fundamental vibrational wavenumbers of MDPO calculated by DFT (B3LYP/6-311++G(d,p) and HF/6-311++G(d,p) given in Table 2. The calculated vibrational wavenumbers, IR intensities, Raman scattering activities and Raman intensities are compared with experimental FT-IR and FT-Raman frequencies as listed in Table 2. Theoretical FT-IR and FT-Raman spectra of MDPO are shown in Figs 2 and 3. The experimental FT-IR and FT-Raman spectra of MDPO are shown in Figs 4 and 5.

Table 2 — Comparison of the experimental (FT-IR, FT-Raman wavenumbers (cm^{-1})) and theoretical wavenumbers (cm^{-1}), infrared intensities (I^{IR}), Raman scattering activities (S^{Ra}) and Raman intensities(I^{RA}) of MDPO calculated by HF/6-311++G(d,p) and B3LYP/6-31++G(d,p) methods

Experimental frequency (cm^{-1})		Calculated frequency (cm^{-1})								Vibrational assignments
		HF/6-311++G(d,p)				B3LYP/6-31++G(d,p)				
FTIR	FT-Raman	Unscaled	I^{IR}	S^{RA}	I^{RA}	Unscaled	I^{IR}	S^{RA}	I^{RA}	
		−68	2.96	0.84	−97.97	−102	2.96	0.59	−46.78	Ring t
	94	96	3.98	0.33	25.52	−85	5.22	1.50	−142.75	Ring ω
		111	1.60	2.87	192.60	74	0.36	1.89	191.67	Butterfly
		129	0.14	2.25	128.78	98	0.28	3.06	233.31	Ring ω
		136	0.33	2.42	130.83	101	0.20	3.20	236.85	C-N ω
	190	175	0.16	3.61	149.31	136	0.17	3.96	214.45	Ring t
	225	228	0.62	4.94	153.15	189	0.09	4.32	164.77	Ring ω
	248	260	1.70	1.58	42.51	221	3.09	2.33	75.01	Ring ω
	275	281	1.32	0.96	23.74	253	2.35	0.35	9.59	Ring β
	294	302	0.24	0.95	21.53	273	0.37	1.26	31.93	Ring ω
		329	0.48	1.73	35.66	290	3.92	2.62	62.29	C—C ω
		336	5.59	1.79	36.02	298	0.15	1.19	27.52	C—C ω
		373	1.30	4.65	82.74	340	1.21	4.88	96.68	Ring β
		397	2.97	0.22	3.70	356	3.65	1.15	21.61	Ring ω
424		437	2.75	1.44	21.30	390	3.10	3.81	64.35	C—H ω
478		507	2.83	0.50	6.18	454	0.22	0.08	1.07	C—H ω
525	531	514	0.89	0.15	1.87	464	3.73	0.49	6.74	CH_3twis
	553	554	4.60	0.30	3.36	470	1.44	0.39	5.36	CH_3twis
		570	0.52	0.25	2.66	501	6.27	1.23	15.33	C—H ω
598		597	14.38	1.28	12.86	526	10.73	1.90	22.44	C—N β
	619	619	10.96	1.74	16.67	553	5.97	1.16	12.88	C—H ω
		620	0.77	2.46	23.60	566	9.10	1.80	19.30	Ring ω
	642	629	10.92	1.26	11.89	576	1.56	2.48	26.09	Ring β
	669	2.69	4.20	36.51	627	4.18	4.59	43.32	C—C β	
675	676	673	1.34	7.30	62.87	629	0.19	2.48	23.26	C—H ω
		690	2.05	2.69	22.41	632	0.62	4.79	44.79	Ring β
694		699	3.11	4.86	39.80	653	4.83	6.25	56.08	Ring β
	752	733	0.74	2.55	19.60	678	3.17	4.08	34.80	C=O ω
791	793	787	5.10	7.67	53.60	729	13.55	4.25	32.89	C—C ω
		825	13.94	4.19	27.44	750	25.21	2.73	20.38	C—H ω
837		847	11.32	1.86	11.74	768	16.63	1.10	7.95	C—C ω
	871	866	22.14	29.71	181.78	799	41.88	5.46	37.38	C—H ω
	882	2.41	23.99	143.10	820	38.72	1.17	7.73	C—H ω	
922	932	930	78.99	1.01	5.61	830	36.37	9.12	59.24	C—H ω
		938	68.99	0.72	3.95	834	1.41	45.23	291.70	C—H ω
961	960	959	18.66	19.59	103.66	893	58.22	6.01	35.24	N—H ω
		993	0.44	2.48	12.47	907	0.85	3.81	21.87	C—H ω

Contd —

Table 2 — Comparison of the experimental (FT-IR, FT-Raman wavenumbers (cm^{-1})) and theoretical wavenumbers (cm^{-1}), infrared intensities (I^{IR}), Raman scattering activities (S^{Ra}) and Raman intensities(I^{RA}) of MDPO calculated by HF/6-311++G(d,p) and B3LYP/6-31++G(d,p) methods — *Contd*

Experimental frequency (cm^{-1})		Calculated frequency (cm^{-1}) HF/6-311++G(d,p)				B3LYP/6-31++G(d,p)				Vibrational assignments
FTIR	FT-Raman	Unscaled	I^{IR}	S^{RA}	I^{RA}	Unscaled	I^{IR}	S^{RA}	I^{RA}	
		997	0.67	2.83	14.11	912	16.70	9.42	53.63	C—H ω
	1002	1008	0.83	31.32	153.98	931	5.32	5.32	29.35	C—H ω
		1025	6.66	63.95	306.72	945	1.13	15.47	83.53	Ring breathing
1030		1030	10.08	26.25	124.98	964	2.55	3.48	18.26	C—H ω
		1035	30.53	20.73	97.98	972	3.49	20.65	107.13	C—H ω
		1041	5.37	2.75	12.87	979	12.03	136.27	699.59	Ring β
		1054	6.89	3.36	15.44	992	1.68	10.88	54.72	Ring β
1072		1072	2.11	3.19	14.27	1000	1.75	14.83	73.78	C—H ω
		1081	2.25	0.23	1.04	1004	1.62	2.60	12.87	CH_2 rock
		1089	9.65	2.71	11.87	1012	17.26	10.24	50.04	Ring β
		1094	1.61	1.40	6.08	1015	0.13	0.04	0.21	C—H ω
1099		1107	25.37	9.49	40.54	1025	4.48	3.10	14.87	C—H ω
		1120	5.95	0.69	2.90	1027	2.68	0.38	1.81	C—H ω
1142		1142	4.88	2.55	10.37	1034	0.40	0.18	0.84	C—H ω
		1144	0.66	5.14	20.86	1048	7.31	9.98	46.27	C—N ν
		1151	18.99	3.66	14.75	1068	8.37	2.32	10.47	C—C ν
		1153	7.11	1.19	4.78	1077	5.60	0.25	1.15	C—C ν
		1158	0.61	0.24	0.98	1097	1.07	1.24	5.39	C—N ν
		1164	0.12	0.16	0.64	1122	2.88	4.40	18.39	CH_3δ rock
		1183	2.41	8.27	31.87	1140	11.39	2.89	11.80	CH_3ω
1223		1220	2.47	2.16	7.93	1160	2.57	1.68	6.67	C—H β
		1239	8.45	3.05	11.03	1163	0.62	1.12	4.44	C—C ν
		1255	1.37	8.18	28.64	1174	1.82	9.98	38.87	C—C ν
1273		1267	0.23	0.77	2.67	1188	34.85	12.93	49.42	C—Hβ
		1291	32.58	3.10	10.37	1194	7.00	5.80	22.00	C—Hβ
		1295	12.37	5.45	18.17	1201	3.49	6.18	23.23	CH_3 α rock
		1299	2.43	9.45	31.29	1218	3.68	12.52	46.04	C—C ν
		1314	2.19	4.71	15.33	1238	7.07	22.87	81.88	C—C ν
		1331	6.08	8.01	25.48	1257	4.67	6.96	24.33	CH_2twis
1339	1353	1345	30.19	6.41	20.05	1260	7.85	0.84	2.95	C—C ν
		1374	7.13	6.45	19.48	1269	5.15	9.28	31.93	C—C ν
		1425	8.73	2.21	6.28	1316	4.36	2.97	9.63	C—Hβ
1447	1449	1456	1.50	1.59	4.35	1327	1.09	5.52	17.65	C—Hβ
		1465	6.37	4.57	12.38	1340	8.47	11.95	37.60	CH_2 wag
		1479	0.71	5.28	14.05	1346	1.56	7.18	22.44	C—Hβ
1493		1491	18.57	5.83	15.30	1361	11.21	5.80	17.79	C—H β
		1524	4.59	7.55	19.03	1386	16.04	19.54	58.08	C=O···Hν
		1543	4.49	2.09	5.16	1409	20.00	2.04	5.92	C—H β-pyridine
		1555	19.06	1.75	4.27	1419	10.15	2.61	7.47	C—H β-pyridine
		1560	25.70	1.07	2.60	1446	11.60	17.45	48.29	C—H β
		1580	7.43	1.46	3.45	1450	10.46	0.64	1.77	CH_3 ω-def
1597	1585	1585	5.39	0.61	1.44	1462	1.91	4.26	11.58	C—Hβ
	1602	1614	46.80	7.24	7.40	1471	36.13	9.77	26.23	N—Hβ
		1617	9.37	3.25	7.38	1489	10.30	17.34	45.58	C—H β-pyridine
		1630	10.95	11.93	26.66	1504	14.32	8.00	20.67	CH_2scis
		1631	6.39	3.89	8.68	1512	9.57	2.60	6.66	C—Hβ
		1637	8.18	9.78	21.67	1514	14.86	1.88	4.80	CH_3β
		1645	28.17	2.37	5.22	1516	7.51	11.70	29.77	C—H β
		1660	12.10	9.34	20.16	1518	8.94	8.43	21.42	CH_3 (ip-def)
		1664	6.51	45.82	98.45	1561	5.70	41.13	99.33	C—C ν
		1681	4.26	15.25	32.20	1572	3.77	13.64	32.57	C—H β
1701	1702	1704	6.09	31.36	64.53	1590	8.90	62.22	145.47	C—C ν

Contd—

Table 2 — Comparison of the experimental (FT-IR, FT-Raman wavenumbers (cm^{-1})) and theoretical wavenumbers (cm^{-1}), infrared intensities (I^{IR}), Raman scattering activities (S^{Ra}) and Raman intensities(I^{RA}) of MDPO calculated by HF/6-311++G(d,p) and B3LYP/6-31++G(d,p) methods — *Contd*

Experimental frequency (cm^{-1})		Calculated frequency (cm^{-1})								Vibrational assignments
		HF/6-311++G(d,p)				B3LYP/6-31++G(d,p)				
FTIR	FT-Raman	Unscaled	I^{IR}	S^{RA}	I^{RA}	Unscaled	I^{IR}	S^{RA}	I^{RA}	
		1714	16.78	25.61	52.07	1591	5.55	16.44	38.37	C—C ν
1886		1872	295.52	17.84	30.56	1811	16.34	2.35	4.32	H···H ν
1952		1958	15.00	2.28	3.57	1853	226.08	16.91	29.59	C=O ν
2928	2930	2930	10.50	389.90	232.75	2813	8.78	1182.30	790.01	C—H ν-pyridine
		2933	24.48	109.02	64.89	2883	24.33	135.65	84.72	C—H sym ν –methyl
		2955	2.22	177.56	103.49	2889	8.82	33.97	21.09	C—H sym ν-(CH_2)
		2957	35.49	78.05	45.44	2904	20.78	114.07	69.87	C—H ν-pyridine
		2959	23.97	245.76	142.68	2907	12.70	46.96	28.69	C—H ν-pyridine
2974	2975	2986	35.46	66.86	37.83	2948	2.52	97.03	56.94	C—H asym ν-(CH_2)
	2996	16.51	64.16	35.99	2949	27.77	26.77	15.70		C—H asymν-(CH_3)
3028	3044	2998	34.50	54.34	30.39	2959	20.30	59.93	34.80	C—H asym ν-(CH_3)
3063	3059	3100	2.43	32.42	16.46	3041	10.85	18.06	9.70	C—H asymν-phenyl
		3101	1.59	34.37	17.43	3054	1.96	36.42	19.32	C—H asym ν-phenyl
		3109	2.75	141.88	71.41	3056	0.78	54.20	28.69	C—H asym ν-phenyl
		3110	13.18	85.49	42.99	3061	1.97	131.94	69.51	C—H asym ν-phenyl
		3118	22.59	39.67	19.80	3064	3.35	117.03	61.46	C—H asym ν-phenyl
		3118	13.93	72.79	36.29	3069	21.47	63.10	32.99	C—H asym ν-phenyl
		3125	16.98	14.85	7.36	3073	25.66	58.05	30.24	C—H asym ν-phenyl
		3126	23.62	15.58	7.71	3076	21.85	21.07	10.94	C—H asym ν-phenyl
		3133	24.64	313.79	514.35	3082	22.95	337.59	174.31	C—H sym ν-phenyl
3167		3134	13.21	330.91	162.62	3083	14.11	404.30	208.56	C—H sym ν-phenyl
3522	3298	3530	4.19	59.29	19.92	3492	2.16	77.32	26.94	N—H ν

ω, out-of-plane bending; β, in-plane-bending; t,torsion; twis, twisting; rock, rocking;ν, stretching; δ rock, out-of-plane rocking; α rock, in-plane-rocking; wag-wagging; scis, scissoring; ip-def, in-plane deformation; sym ν, symmetric stretching; asym ν, asymmetric stretching

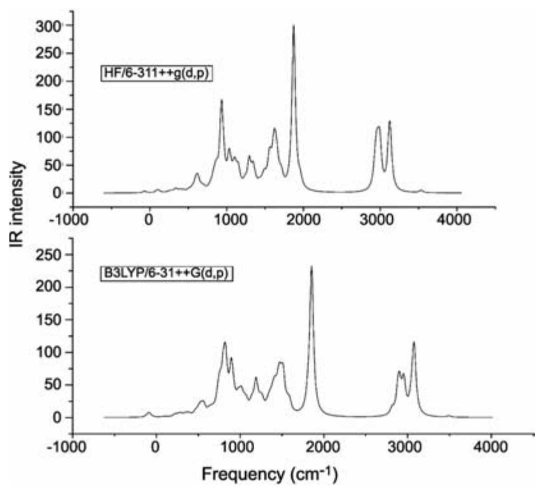

Fig. 2 — Theoretical IR intensity spectrum of MDPO

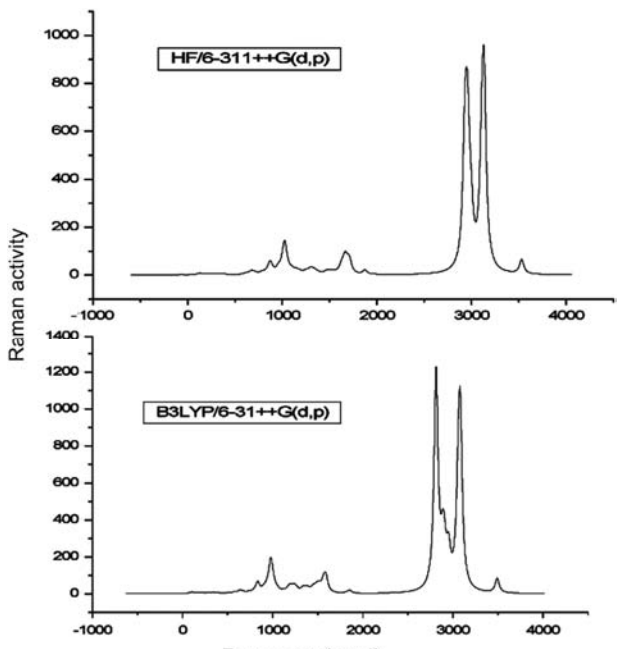

Fig. 3 — Theoretical Raman Activity spectrum of MDPO

4.2.1 N-H vibrations

The N–H stretching vibration[17, 18]appears strongly and broadly in the region 3500-3300 cm^{-1}. Erdogdu *et al*[19]. assigned N–H stretching mode in the region 3500-3300 cm^{-1}.In this study, the peak was observed

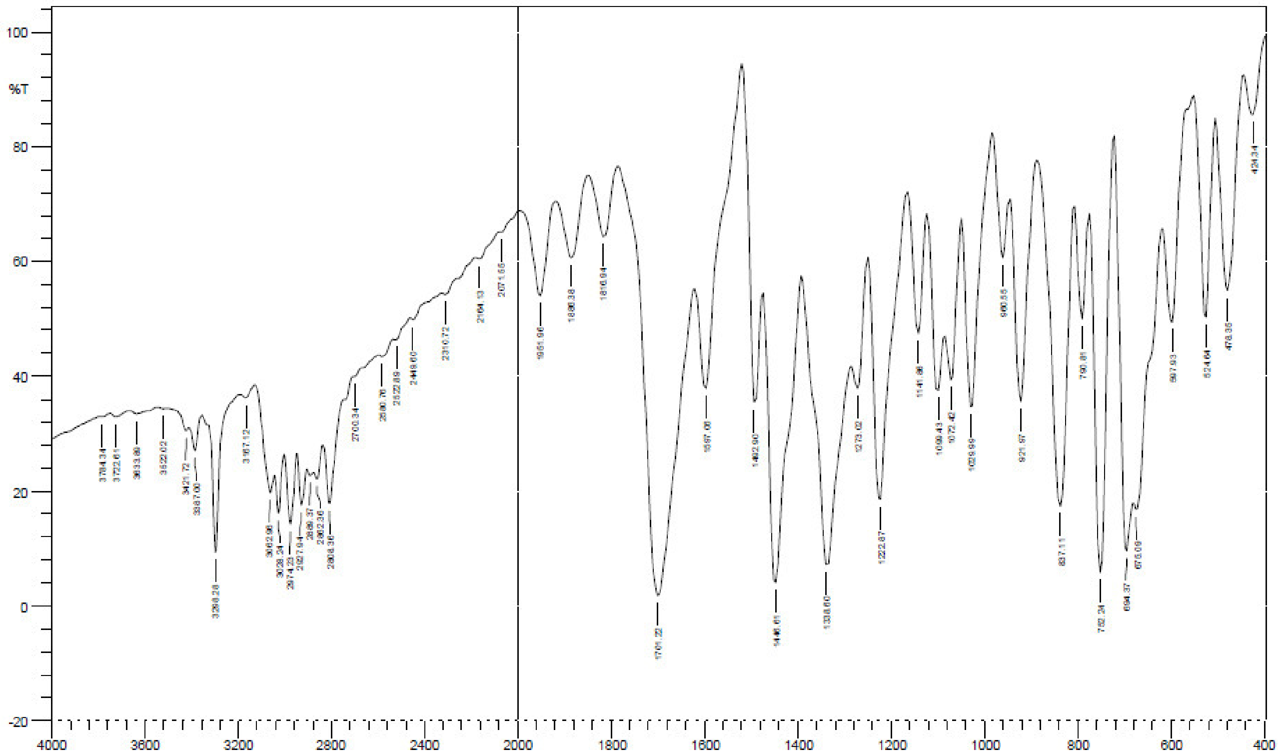

Fig. 4 — FT-IR Experimental spectrum of MDPO

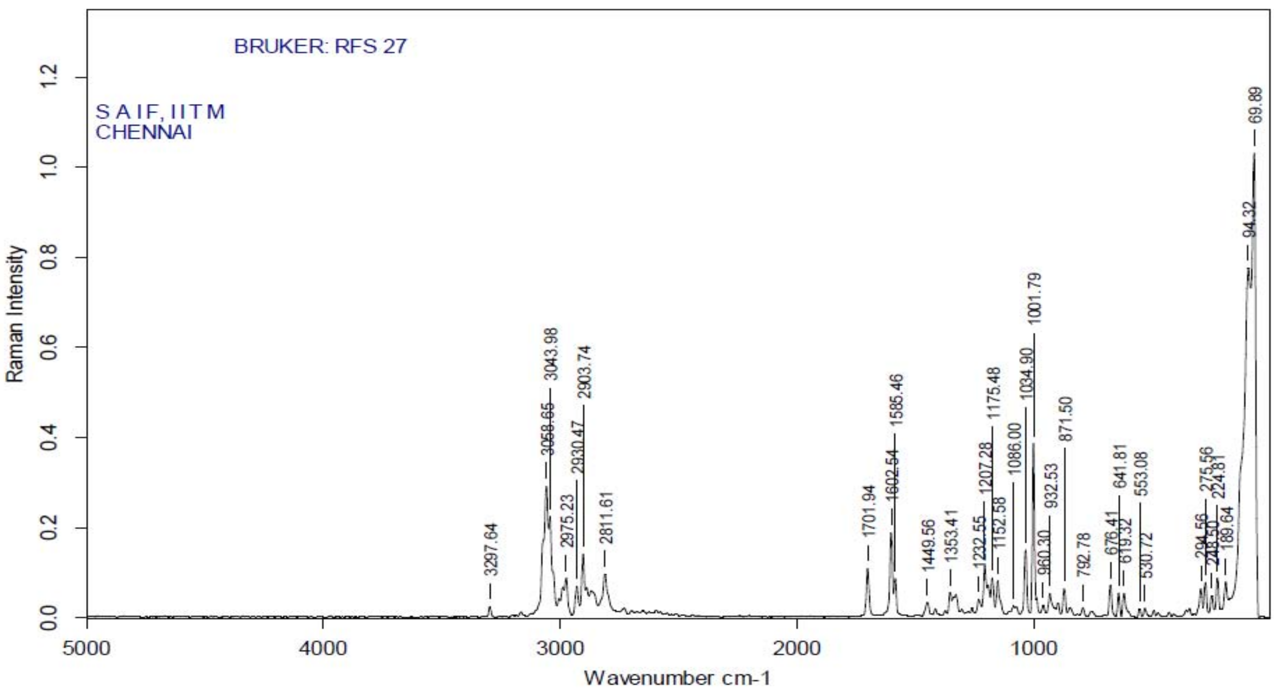

Fig. 5 — FT-Raman Experimental spectrum of MDPO

as medium and narrow band in FT-IR, but weak and narrow bands in FT-Raman, where the peaks are attributed to 3387 cm^{-1} and 3298 cm^{-1} for FT-IR and FT-Raman, respectively. The corresponding theoretical peak for N–H stretching mode is about 3492 cm^{-1} in B3LYP/6-311++G (d, p) basis set and 3530 cm^{-1} in HF/6-311++G (d, p) basis set which shows positive deviation from the experimental value. The N–H stretching fundamental of piperidine was observed in the vapour phase[20] at 3364 cm^{-1}. The position of the methyl group in the piperidine ring influences the N–H stretching wavenumber. Out-of-plane bending modes (N–H) is calculated at 892 cm^{-1}. This vibration is in agreement with the observed FT-IR (921 cm^{-1}) and FTRaman (871 cm^{-1}) bands.

4.2.2 CH_3 and CH_2 group vibrations

Methyl groups are, generally, referred to as electron donating substituents in the aromatic ring system[21]. In acetates, the asymmetric vibrations of the methyl group are expected to occur in the region 2940-3040 cm^{-1} and symmetric vibrations are in the region 2910-2930 cm^{-1}, and usually the bands are weak[22]. Aromatic acetyl substituent absorbs in a narrow range 3000-3020 cm^{-1} and the absorption sometimes coincides with a C–H stretching mode of the ring. The title molecule possesses methyl (CH_3) and methylene (CH_2) groups. For the assignments of CH_3 group frequencies, basically, nine fundamentals can be associated to CH_3 group namely, CH_3sym, symmetric stretch, CH_3asym, asymmetric stretch,CH_3 ipscis, in-plane scissoring.CH_3op scis, out-of-plane scissoring, CH_3ip bend, in-plane bending, CH_3 op bend, out-of-plane bending, CH_3ip twist, in-plane twisting, CH_3 op twist, out-of plane twisting and CH_3 torsion modes. Methyl in-plane deformations occur theoretically at 1518 and 1450 cm^{-1} wavenumbers and methyl in-plane bending at 1514 cm^{-1}. These two vibrations have experimental support at 1492 cm^{-1} in FT-IR and at 1449 cm^{-1} in FT-Raman spectra. Methyl out-of-bending vibration is predicted at 1122 and 1140 cm^{-1}. The corresponding sharp peaks were found experimentally at 1141 cm^{-1} in FT-IR and at 1152 cm^{-1} in FT-Raman spectra. The methyl twisting predicted theoretically at 464 and 470 cm^{-1} has a sharp peak at 478 cm^{-1} in FT-IR spectrum.

For the assignments of CH_2 group frequencies, basically six fundamentals can be associated to each CH_2 group namely, CH_2sym, symmetric stretch, CH_2asym, asymmetric stretch, CH_2scis, scissoring and CH_2 rock, rocking modes which belong to polarized in-plane vibrations. In addition to that CH_2 wag, wagging and CH_2 twist, twisting modes of CH_2 group would be expected to be depolarized for out-of-plane bending vibrations. The C–H stretching vibrations of the methylene group are at lower frequencies than those of the aromatic C–H ring stretching. The asymmetric CH_2 stretching vibration is, generally, observed in the region 3000-2900 cm^{-1}, while the CH_2 symmetric stretching will appear between 2900 and 2800 cm^{-1} (Ref. 23). In the present study, it is evident for C–H symmetric stretching of mehthylene group at 2889 cm^{-1} and for C–H asymmetric stretching of methylene group at 2948 cm^{-1}. The CH_2 symmetric stretching vibrations are observed at 2889 cm^{-1} in FT-IR and at 2903 cm^{-1} in FT-Raman spectra. The CH_2 asymmetric stretching vibrations are observed at 2927 cm^{-1} in FT-IR and at 2930 cm^{-1} in FT-Raman spectra. In the present assignment, the CH_2 bending modes follow in decreasing wavenumber with the general order CH_2 scissoring > CH_2 wagging > CH_2 twist> CH_2 rock. The computed wavenumber of 1504 cm^{-1} for CH_2 scissoring is in line with peak at 149 2 cm^{-1} in FTIR spectrum. For CH_2 wagging, calculated value of 1340 cm^{-1} is in line with strong peak at 1338 cm^{-1} in FT-IR and medium peak at 1353 cm^{-1} in FT-Raman spectra. CH_2 twisting calculated at 1257 cm^{-1} is in line with weak bands at 1273 cm^{-1} in FT-IR and at 1232 cm^{-1} in FT-Raman spectra.CH_2 rocking calculated at 1004 cm^{-1} is in line with peak at 1001 cm^{-1} in FT-Raman spectra.

4.2.3 C=O vibrations

Stretching vibration of carbonyl group C=O can be observed as a very strong band in both FT-IR and FT-Raman spectra[24] at 1665 cm^{-1}. The carbonyl stretching C=O vibration[22] is expected to occur in the region 1715-1680 cm^{-1}. The deviation of the calculated wavenumbers for this mode can be attributed to the underestimation of the large degree of π-electron delocalization due to conjugation of the molecule. In the present paper, we have observed stretching vibrations of C=O at 1338. 1701 and 1886 cm^{-1} in FT-IR. with 1701 cm^{-1} being very strong band and at 1353 and 1701 cm^{-1} in FT-Raman, the latter being strong band. The computed frequencies are 1386 and 1853 cm^{-1} for C=O stretching vibrations. C=O out-of-plane bending is computed at 678 cm^{-1}. The experimental peaks at 675 and 694 cm^{-1} in FT-IR spectrum and at 676 cm^{-1} in FT-Raman spectrum are in line with the computed value.

4.2.4 C-N vibrations

The identification of C–N vibration is a very difficult task, since mixing of several bands are possible in this region. In the gas phase spectrum of the piperidine molecule Vedal *et al*[20]. observed the C–N stretching at 1147 and 1313 cm^{-1} and in solid state piperidine molecule Gulluoglu *et al*[25]. observed the C–N stretching at 1135 and 1317 cm^{-1}. The theoretical wavenumbers for C–N stretching vibrations in this title molecule are 1048 and 1097 cm^{-1}. The C-N in-plane and out-of plane bending vibrations are at 100 and 526 cm^{-1}. respectively. The experimental peak values that are in line with theoretical wavenumbers are (FT-IR: 1029 and 1099 cm^{-1}, FT-Raman: 1034 and 1086 cm^{-1}) for C–N stretching vibrations. C-N in-plane bending vibrations calculated at 526 cm^{-1} has experimental peaks at 530 cm^{-1} in FT-Raman and at 524 cm^{-1} in FT-IR spectra. C-N out-of-plane bending vibration predicted at 100 cm^{-1} has experimental peak at 94 cm^{-1} in FT-Raman spectrum only. The C-N stretching vibration[22] normally appears around 1300 cm^{-1}. In the present work, the C–N stretching frequencies are reasonably lowered.

4.2.5 C-C vibrations

The carbon–carbon stretching modes of the pyridine are expected in the range 1650-1100 cm^{-1} which are not significantly influenced by the nature of the substituents[26]. The C–C stretching vibrations of phenyl ring and methylene are calculated in the range 1591–1068 cm^{-1}. These vibrations are in line with experimental values (1072, 1099, 1141, 1222, 1273 and 1597 cm^{-1} in FT-IR and 1086, 1152, 1175, 1207, 1232 and 1585 cm^{-1}in FT-Raman). C-C out-of-plane bending vibrations are theoretically calculated at 290, 297, 729 and 768 cm^{-1} and C-C in-plane bending vibration is calculated at 626 cm^{-1}which are found to be in agreement in both IR and Raman experimental spectra.

4.2.6 C–H vibrations

The C–H stretching modes of the ring and methyl group were observed at 2730 cm^{-1}, 2800 cm^{-1}, 2868 cm^{-1} and 2920 cm^{-1} for 3-methylpiperidine[27]. The C–H stretching modes were predicted in the range 2813-3083 cm^{-1}. One can also expect C–H stretching vibrations for the title molecule as a very strong band in FTRaman spectrum at 2811, 2903, 2930, 2975, 3043 and 3058 cm^{-1} and strong FT-IR bands at 2808, 2862, 2889, 2927, 2974, 3028 and 3062 cm^{-1}. are assigned to C–H stretching vibration. The theoretically computed wavenumbers from 2813 to 3083cm^{-1} show good agreement with the recorded spectra.Vedal *et al*[20]. assigned the C–H stretching vibration in piperidine molecule at 2925 cm^{-1} in gas phase spectrum, Gulluoglu *et al*[25]. assigned the C–H stretching vibration in piperidine molecule by B3LYP/6-31G (d) method at 2911 cm^{-1}. The theoretical results show that the computed value by B3LYP/6-311++G(d,p) method is in good agreement with the literature value. The C–H in-plane bending modes of vibrations are assigned for the wavenumbers in the range 1160-1572 cm^{-1}. The lower experimental peaks in support to this range are 1141, 1338, 1446 and 1492 cm^{-1} in FT-IR and 1152, 1175, 1353 and 1449 cm^{-1} in FT-Raman spectra. The C-H out-of-plane bending modes of vibration are assigned for the wavenumbers in the range 390-1034 cm^{-1}. The extreme lower experimental peaks in support to this range are 478, 524, 597, 694, 752, 837, 921 and 960 cm^{-1} in FT-IR and 553, 619, 641,792, 932, 960, 1001 cm^{-1} in FT-Raman spectra.

4.2.7 Ring vibrations

These modes are not pure but they contribute drastically from other vibrations and are substituent-sensitive. In the title molecule, ring in-plane and out-of-plane bending modes are affected to a great extent by the substituents and produce bands below 660 cm^{-1} and few bands near 1000 cm^{-1}. The calculated theoretical wavenumbers of ring torsion, ring in-plane bending, ring out-of plane bending, ring breathing and butterfly vibrational modes are discussed here. The only ring torsion effect is observed at 136 cm^{-1}. Ring in-plane bending vibrations are assigned at 252, 339, 575, 631, 652, 978, 992 and 1012 cm^{-1}.Ring out-of-plane bending vibrations are assigned at 98, 188, 273, 355 and 566 cm^{-1}. A peculiar ring vibration called butterfly vibration mode observed at 74 cm^{-1} is because of both the phenyl rings approach and recede alternatively. The peaks for these modes are not observed in FT-IR spectrum since these modes are possible to appear only in far IR spectrum. The weak intensity bands present at 189 and 275 cm^{-1} in FT-Raman spectrum are assigned to ring out-of-plane bending. The medium intensity band 641 cm^{-1} and a strong band at 1001 cm^{-1} in FT-Raman spectrum are assigned to ring in-plane bending. The theoretical wavenumbers corresponding to ring vibrations are found to have agood correlation with the available experimental observations.

5 UV Analysis

The lowest singlet→singlet spin allowed excited states need to be accounted to investigate the electronic transition[40]. The absorption wavelength, excitation energies and oscillator strength for the title molecule in the solvents methanol, benzene and water are computed using TD/HF-6311++G(d,p) method. The solvent effects on the absorption wavelengths and excitation energies are examined by the Polarizable continuum Model using TD/HF-6311++G(d,p) method. The three absorption peaks of the title molecule have a mean oscillator strength (say ~0.016 au). The simulated theoretical UV-spectrum of MDPO are shown in Figs 6-8. In the electronic spectrum, the strong intensity peaks at the maximum absorption wavelength of (223.74 nm) in methanol), (224.43 nm in benzene) and (223.71 nm in water) are caused by $n \rightarrow \pi^*$ transitions, while the smaller intensity bands calculated near 242 nm in water and methanol and at 246 in benzene phases of the title molecule are forbidden and therefore, the oscillator strengths of these phases nearly equal to zero. The calculated spectra agree with the experimental UV spectra of MDPO with methanol, benzene and water solvents as shown in Figs 6a, 7a and 8a, respectively. UV analysis of 3-methyl-2,6-diphenylpiperidin-4-one is shown in Table 3 with theoretical absorption wavelength λ (nm), excitation energies E (eV) and

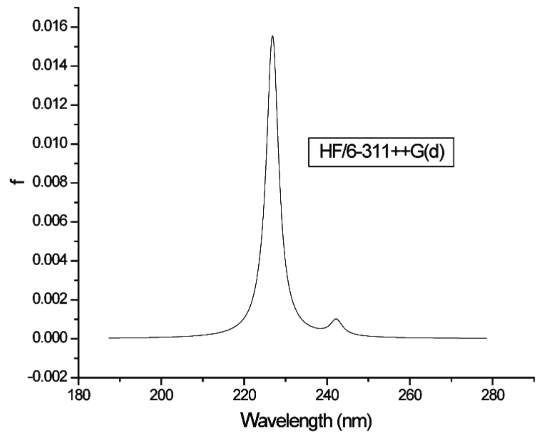

Fig. 6 — Theoretical UV spectrum – methanol solvent in MDPO

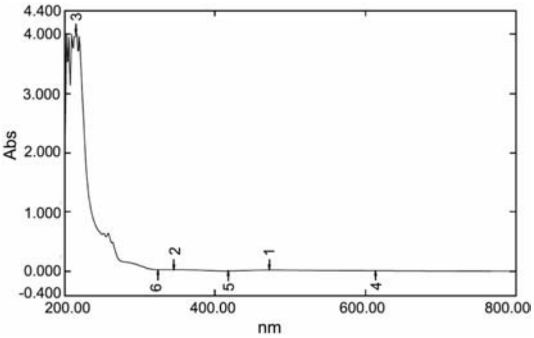

Fig. 6(a)─Experimental UV spectrum – methanol solvent in MDPO

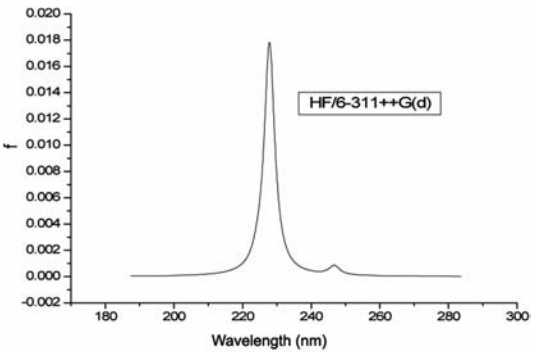

Fig. 7 — Theoretical UV spectrum – benzene solvent in MDPO

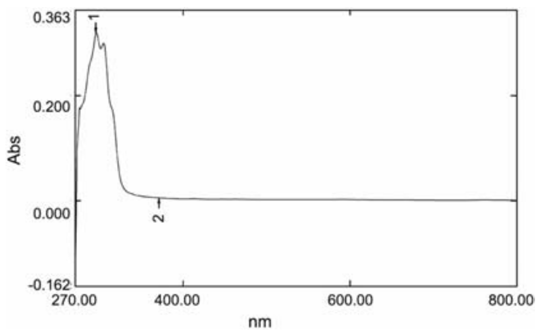

Fig. 7(a) — Experimental UV spectrum – methanol solvent in MDPO

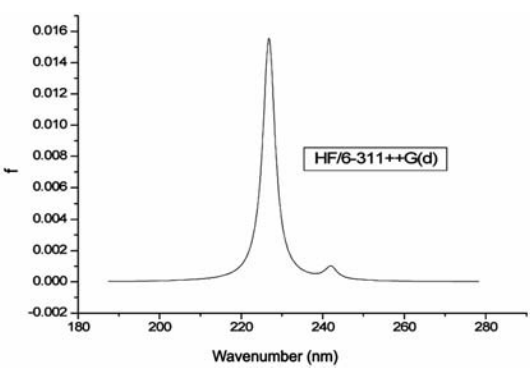

Fig. 8 — Theoretical UV spectrum – water solvent in MDPO

oscillator strengths (f) using TD-DFT/B3LYP/6-311++G(d,p) method in solvents such as methanol, benzene and water.

6 Mulliken Charge Distribution

The Mulliken charge is directly related to the vibrational properties of the molecule, and quantifies how the electronic structure changes under atomic displacement; it is therefore, related directly to the chemical bonds present in the molecule. It affects dipole moment, polarizability, electronic structure and more properties of molecular systems. The Mulliken and natural charge distribution of the molecule are calculated for MDPO on HF and B3LYP levels with 6-311++G(d,p) basis set in HF and B3LYP methods. The calculated values of the charges of title molecule are given in Table 4. Distribution of positive and negative charges is vital in increasing or decreasing of bond length between atoms. The charge changes with basis set presumably occurs due to polarization. Considering the two methods of basis set used in the atomic charge calculation, the oxygen atoms exhibit a negative charge, which are donor atoms. The charges of N_1, C_3, C_9 and C_{15} are positive in HF and B3LYP methods with 6-311++G(d,p) basis set. In the case of C_2 and C_6, the charges are positive in HF method with 6-311++G(d,p) basis set and negative in B3LYP method with 6-311++G(d,p) set, but in the case of C_{20}, the charges are negative in HF method with 6-311++G(d,p) basis set and positive in B3LYP method with 6-311++G(d,p) basis set. The rest of the carbon atoms have negative charge. Moreover, positive charge distribution is observed in the remaining 19 hydrogen atoms (H_{21} to H_{39}). Oxygen O_7 is negative in both methods with the largest value of

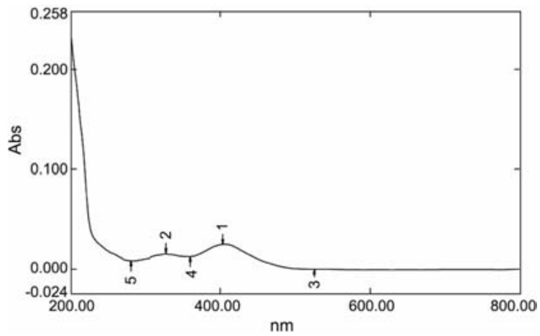

Fig. 8(a) — Experimental UV spectrum – methanol solvent in MDPO

Table 4 — Mulliken atomic charges

Atom type	HF 6-311++G(d,p)	B3LYP 6-311++G(d,p)
N_1	0.008139	0.217646
C_2	0.114943	−1.530317
C_3	0.068334	0.417109
C_4	−0.065584	−0.535547
C_5	−0.901323	−0.733911
C_6	0.065610	−0.640542
O_7	−0.307305	−0.278934
C_8	−0.614776	−1.194469
C_9	0.301647	0.134169
C_{10}	−0.233714	−0.441500
C_{11}	−0.438648	−0.379062
C_{12}	−0.435560	−0.314956
C_{13}	−0.261763	−0.181896
C_{14}	−0.077237	−0.045208
C_{15}	0.786042	0.988742
C_{16}	−0.160299	−0.546005
C_{17}	−0.257254	−0.440348
C_{18}	−0.571342	−0.335386
C_{19}	−0.463365	−0.365023
C_{20}	−0.371770	0.324660
H_{21}	0.279487	0.382510
H_{22}	0.249559	0.347794
H_{23}	0.169673	0.342290
H_{24}	0.242977	0.351487
H_{25}	0.217353	0.307416
H_{26}	0.176733	0.275339
H_{27}	0.177649	0.272839
H_{28}	0.188983	0.295927
H_{29}	0.136546	0.243606
H_{30}	0.184972	0.310894
H_{31}	0.211269	0.287764
H_{32}	0.187962	0.270829
H_{33}	0.214887	0.288590
H_{34}	0.229141	0.346076
H_{35}	0.181403	0.313050
H_{36}	0.224594	0.298996
H_{37}	0.180789	0.270631
H_{38}	0.223452	0.291610
H_{39}	0.176567	0.383129

Table 3 — Theoretical electronic absorption spectra (UV) of MDPO (absorption wavelength λ (nm), excitation energies *E* (eV) and oscillator strengths (f)) using TD-DFT/B3LYP/6-311++G(d,p) method

Excitation states	Methanol			Benzene			Water		
	λ (nm)	Δ*E*(eV)	*f* (a.u.)	λ (nm)	Δ*E*(eV)	*f* (a.u.)	λ (nm)	ΔE(eV)	*f* (a.u.)
Excitated state 1	242.25	5.1180	0.0008	246.74	5.0250	0.0008	242.00	5.1233	0.0008
Excitated state 2	226.84	5.4658	0.0155	227.84	5.4417	0.0155	226.81	5.4664	0.0155
Excitated state 3	223.74	5.5414	0.0002	224.43	5.5245	0.0002	223.71	5.5422	0.0002

−0.30731 a.u in HF method with 6-311++G(d,p) basis set. The atomic charges of carbon, nitrogen and oxygen are presented in Table 4.

7 Thermodynamic Properties

The values of some thermodynamic parameters such as zero point vibrational energy, thermal energy, specific heat capacity, rotational constants, entropy, and dipole moment of MDPO by DFT/B3LYP with 6-31++G(d,p) basis set and HF method with/6-311++G(d,p) basis set are listed in Table 5. The global minimum energy(SCF) obtained for structure optimization of MDPO with 6-311++G(d,p) basis set is −827 au for DFT/B3LYP. The minimum energy becomes −822 au for HF/6-311G++ (d,p) basis set. The difference in amount of energy between the methods is ca. 5 au only. The rotational constant values are observed to be the same in both basis sets of HF and B3LYP methods. The variation in zero-point vibrational energies (ZPVEs) seems to be significant. The biggest value of ZPVE of MDPO is 218.596 kcal mol^{-1} obtained at HF/6-311++G(d,p), whereas the smallest value is 206.665 kcal mol^{-1} obtained at B3LYP/6-311++G(d,p).

Dipole moment reflects the molecular charge distribution and is given as a vector in three dimensions. Therefore, it can be used as descriptor to depict the charge movement across the molecule. Direction of the dipole moment vector in a molecule depends on the centres of positive and negative charges. Dipole moments are strictly determined for neutral molecules. For charged systems, its value depends on the choice of origin and molecular orientation. As a result of HF and DFT (B3LYP) calculations, the highest dipole moment(4.2137D) was observed for HF/6-311G++(d,p), whereas the smallest one(3.6836D) was observed for B3LYP/6-31++G(d,p) in MDPO.

8 HOMO-LUMO

Molecular orbitals (HOMO and LUMO) and their properties such as energy are very useful for physicists and chemists and are very important parameters for quantum chemistry. This is also used by the frontier electron density for predicting the most reactive position in π-electron systems and also explains several types of reaction in conjugated system[28]. Both the highest occupied molecular orbital (HOMO) and lowest unoccupied molecular orbital (LUMO) are the main orbitals taking part in chemical stability. The frontier molecular orbitals play an important role in the electric and optic properties, as

Table 5 — Theoretically computed zero point vibrational energy (kcal mol^{-1}), rotational constants (GHz), rotational temperature (K), thermal energy (kcal mol^{-1}), molar capacity at constant volume (cal mol^{-1} K^{-1}) entropies (cal mol^{-1} K^{-1})

Parameters	HF/6-311++G(d,p)	B3LYP/6-311++G(d,p)
Self-consistent field energy(a.u.)	−822.08672	−827.30191
Zero-point vibrational energy	218.596	206.665
Rotational temperature	0.02273	0.02273
	0.01302	0.01302
	0.00940	0.00940
Rotational constants	0.47372	0.47372
	0.27129	0.27129
	0.19579	0.19579
Energy		
Translational	0.889	0.889
Rotational	0.889	0.889
Vibrational	224.980	213.562
Total	226.757	215.340
Molar capacity at constant volume		
Translational	2.981	2.981
Rotational	2.981	2.981
Vibrational	50.464	54.539
Total	56.426	60.501
Entropy		
Translational	42.625	42.625
Rotational	33.812	33.812
Vibrational	35.556	38.890
Total	111.993	115.327
Dipole moment	4.2137	3.6836

well as in UV-Vis spectra and chemical reactions. The analysis of the wave function indicates that the electron absorption corresponds to the transition from the ground to the first excited state and is mainly described by one electron-excitation from the highest occupied molecular orbital (HOMO) to the lowest unoccupied orbital (LUMO). The bioactivity and chemical activity of the molecule depends on eigen value of HOMO, LUMO and energy gap. HOMO as an electron donor represents the ability to donate an electron. LUMO as an electron acceptor represents the ability to obtain an electron. The energy of HOMO is directly related to the ionization potential, and that of LUMO is directly related to electron affinity. The energy difference between the HOMO and LUMO is about 4.9427 eV. The smaller band gap increases the stability of the molecule.The frontier molecular orbitals are shown in Figs 9 and 10. The HOMO and LUMO energy calculated by B3LYP/6-311++G(d,p) method in gas phase is given below.

HOMO energy (B3LYP) = −6.1179 eV
LUMO energy (B3LYP) = −1.1752eV
HOMO − LUMO energy gap (B3LYP) = 4.9427 eV

9 NBO Analysis

9.1 Natural Population Analysis

The natural population analysis performed on the electronic structure of title molecule clearly describes the distribution of electrons in various sub-shells of their atomic orbitals. The accumulation of charges on the individual atom and accumulation of electrons in the core, valence and Rydberg sub-shells of MDPO are presented in Table 6.The most electronegative atoms like N_1, O7 and C_8 have charges −0.69074, −0.61686 and −0.52510. respectively. The most electropositive atom is C_4 with charge 0.66144. From the electrostatic point of view, electronegative atoms have a tendency to donate an electron, whereas the electropositive atoms have a tendency to accept an electron. Further, natural population analysis showed that 142 electrons in the title compound are distributed on the sub-shells as follows:

Core: 39.9854 (99.9637% of 40)
Valence: 101.6257 (99.6331% of 102)
Rydberg : 0.38873 (0.2738 % of 142)

9.2 Natural Atomic Orbitals

The occupancies and energies of lone pair molecular orbitals (LP) and anti-bonding (BD^*) molecular orbitals of the MDPO are predicted at HF/6-311++G level of theory and is presented in Table 7. The variations in occupancies and energies of the title molecule directly give the evidence for the delocalization of charge upon substitution and this leads to the variation of bond lengths.

9.3 Natural Bond Orbital Analysis

The interactions result in a loss of occupancy from the localised NBO of the idealized Lewis structure into an empty Non-Lewis orbital. NBO analysis of some pharmaceutical compounds has been performed by many spectroscopists[37-39]. The lone pair-anti-bonding interaction can be quantitatively described by

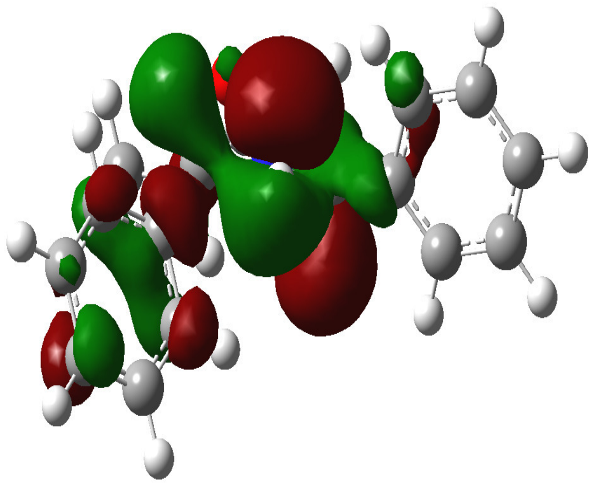

HOMO = −6.1179 eV

Fig. 9 — HOMO Plot of MDPO

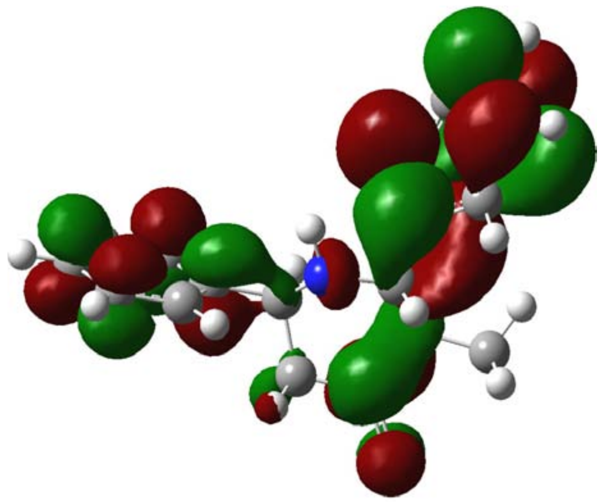

LUMO = −1.1752eV

Fig. 10 — LUMO Plot of MDPO, ΔE = 4.9427 eV

Table 6 — Accumulation of natural charges population of electrons in core, valence and Rydberg orbitals of MDPO

Atom	Charge	Natural Population			Total
		Core	Valence	Rydberg	
N_1	−0.69074	1.99955	5.67550	0.01569	7.69074
C_2	−0.00802	1.99919	3.98431	0.02452	6.00802
C_3	−0.30023	1.99917	4.28683	0.01423	6.30023
C_4	0.66144	1.99934	3.30135	0.03787	5.33856
C_5	−0.45025	1.99927	4.43582	0.01516	6.45025
C_6	−0.05376	1.99915	4.02929	0.02532	6.05376
O_7	−0.61686	1.99977	6.60613	0.01096	8.61686
C_8	−0.52510	1.99947	4.51646	0.00917	6.52510
C_9	−0.03049	1.99913	4.01252	0.01883	6.03049
C_{10}	−0.20370	1.99918	4.18895	0.01557	6.20370
C_{11}	−0.19542	1.99928	4.17765	0.01849	6.19542
C_{12}	−0.21226	1.99928	4.19456	0.01843	6.21226
C_{13}	−0.19087	1.99928	4.17334	0.01825	6.19087
C_{14}	−0.19738	1.99918	4.18237	0.01584	6.19738
C_{15}	−0.03966	1.99910	4.02357	0.01700	6.03966
C_{16}	−0.19644	1.99918	4.17976	0.01750	6.19644
C_{17}	−0.19295	1.99928	4.17524	0.01843	6.19295
C_{18}	−0.20589	1.99928	4.18839	0.01821	6.20589
C_{19}	−0.18278	1.99925	4.16581	0.01772	6.18278
C_{20}	−0.26257	1.99915	4.24604	0.01737	6.26257
H_{21}	0.36029	0.00000	0.63847	0.00124	0.63971
H_{22}	0.19874	0.00000	0.79975	0.00151	0.80126
H_{23}	0.22161	0.00000	0.77691	0.00148	0.77839
H_{24}	0.24164	0.00000	0.75667	0.00168	0.75836
H_{25}	0.19444	0.00000	0.80453	0.00103	0.80556
H_{26}	0.19987	0.00000	0.79587	0.00426	0.80013
H_{27}	0.20543	0.00000	0.79347	0.00111	0.79457
H_{28}	0.19945	0.00000	0.79957	0.00098	0.80055
H_{29}	0.18204	0.00000	0.81713	0.00084	0.81796
H_{30}	0.20399	0.00000	0.79507	0.00094	0.79601
H_{31}	0.20450	0.00000	0.79468	0.00081	0.79550
H_{32}	0.20517	0.00000	0.79407	0.00076	0.79483
H_{33}	0.20581	0.00000	0.79338	0.00082	0.79419
H_{34}	0.22115	0.00000	0.77771	0.00114	0.77885
H_{35}	0.20573	0.00000	0.79329	0.00098	0.79427
H_{36}	0.20709	0.00000	0.79212	0.00079	0.79291
H_{37}	0.20733	0.00000	0.79191	0.00076	0.79267
H_{38}	0.20641	0.00000	0.79281	0.00078	0.79359
H_{39}	0.22323	0.00000	0.77450	0.00227	0.77677
Core	39.9854	99.9637% of 40			
Valence	101.6257	99.6331% of 102			
Rydberg	0.38873	0.2738% of 142			

the second-order perturbation interaction[29-32] energy $E(2)$**.** For each donor (i) and acceptor (j), the stabilisation energy $E(2)$ associated with the delocalization i→j is estimated as :

$$E(2) = \Delta E_{ij} = q_i \frac{F(ij)^2}{\varepsilon_j - \varepsilon_i}$$

where q_i is the donor orbital occupancy, ε_I and ε_j are the diagonal elements and $F(i,j)$ is the off diagonal NBO Fock matrix element. The NBO analysis provides an efficient method for studying intermolecular and intramolecular bonding. It also provides a convenient basis for intermolecular charge transfer (ICT) or conjugative interactions in molecular system. Table 8 presents the second order perturbation energies (often called as stabilizations energies or interaction energies) of most interacting NBO of MDPO. The second order perturbation energies correspond to the hyper conjugative interactions of title compound such as LP (2) O7→$BD^*(1)C_3$-C_4 and LP(2)O_7→$BD^*(1)C_4$-C_5 that

Table 7 — Occupancies and energies of lone pair orbitals (LP) and anti-bonding (BD^*) molecular orbitals of MDPO

Atomic orbitals	Occupancies	Energies(au)
$LP(1)N_1$	1.93438	−0.47912
$LP(1)O_7$	1.97572	−0.92741
$LP(2)O_7$	1.92613	−0.45584
$BD^*(1)N_1—C_2$	0.02236	0.59243
$BD^*(1)N_1—C_6$	0.02414	0.59360
$BD^*(1)N_1—H_{21}$	0.01343	0.64034
$BD^*(1)C_2—C_3$	0.02783	0.60872
$BD^*(1)C_2—C_{15}$	0.02999	0.65893
$BD^*(1)C_2—H_{22}$	0.01966	0.58345

Table 8 — Second order perturbation theory analysis of Fock matrix in NBO basis (MDPO)

Donor (i)	→	Acceptor (j)	$E^{(2)}$ kJ mol^{-1}	E(j) − E(i) a.u.	F(i,j) a.u.
LP N_1(1)	→	$BD^*(1)$ $C_2—C_3$	2.48	1.09	0.047
LP N_1(1)	→	$BD^*(1)$ $C_2—C_{15}$	8.73	1.14	0.090
LP N_1(1)	→	$BD^*(1)$ $C_2—H_{22}$	1.10	1.06	0.031
LP N_1(1)	→	$BD^*(2)$ $C_4—O_7$	3.10	0.69	0.041
LP N_1(1)	→	$BD^*(1)$ $C_5—C_6$	2.42	1.09	0.046
LP N_1(1)	→	$BD^*(1)$ $C_6—H_{26}$	9.16	1.10	0.090
LP N_1(1)	→	$BD^*(2)$ $C_{15}—C_{16}$	1.43	0.63	0.029
LP O_7(1)	→	$BD^*(1)$ $C_3—C_4$	3.17	1.56	0.063
LP O_7(1)	→	$BD^*(1)$ $C_4—C_5$	1.76	1.55	0.047
LP O_7(2)	→	$BD^*(1)$ $C_3—C_4$	25.73	1.09	0.150
LP O_7(2)	→	$BD^*(1)$ $C_4—C_5$	22.64	1.08	0.141
LP O_7(2)	→	$BD^*(1)$ $C_5—C_6$	0.85	1.07	0.027

are considerably very large with 25.73 and 22.64 kJmol^{-1}, respectively. The interactions such as LP(1) N_1→$BD^*(1)$ C_6-H_{26} and LP (1) N_1→$BD^*(1)$ C_2-C_{15} are little higher than the rest of the interactions as presented in Table 8. These hyper conjugative interactions are the most responsible ones for stability of title compound.

9.4 Electron contribution in s-type and p-type subshells

NBO analysis of title compound is performed to estimate the delocalisation patterns of electron density(ED) from the principal occupied Lewis-type (bond or lone pair) orbitals to unoccupied non-Lewis (anti-bonding or Rydberg) orbitals. The list of occupancies and energies of most interacting NBOs along with their percentage of hybrid atomic orbitals is listed in Table 9. The percentage of hybrid atomic orbitals of oxygen lone pair atom O_7 and nitrogen lone pair atom N_1 shows that O_7 is partially contributed to both s-type and p-type subshells, while N_1 is predominantly contributed to p-type subshell. In contrast, all the anti-bonding orbitals of title compound are mainly contributed to p-type subshell, except in the $BD^*(1)$ C_4-O_7 orbital which shows that O_7 is partially contributed to both s-type and p-type sub-shell, as stated in Table 9.

Table 9 — Natural atomic orbital occupancies of most interacting(lone pair and anti-bonding) NBOs of MDPO

Parameters	Occupancies	Hybrid	AO(%)
LP (1) N_1	1.93438	$sp^{4.39}$	s(18.55) p(81.45)
LP (1) O_7	1.97572	$sp^{0.76}$	s(56.95) p(43.05)
$BD^*(1)$	0.02236	$sp^{2.40}(N_1)$	s(29.41) p(70.59)
$N_1—C_2$		$sp^{3.45}(C_2)$	s(22.45) p(77.55)
$BD^*(1)$	0.02414	$sp^{2.30}(N_1)$	s(30.28) p(69.72)
$N_1—C_6$		$sp^{3.56}(C_6)$	s(21.93) p(78.07)
$BD^*(1)$	0.02783	$sp^{2.75}(C_2)$	s(26.68) p(73.32)
$C_2—C_3$		$sp^{2.68}(C_3)$	s(27.14) p(72.86)
$BD^*(1)$	0.02999	$sp^{2.52}(C_2)$	s(28.43) p(71.57)
$C_2—C_{15}$		$sp^{2.13}(C_{15})$	s(31.97) p(68.03)
$BD^*(1)$	0.05258	$sp^{3.03}(C_3)$	s(24.81) p(75.19)
$C_3—C_4$		$sp^{1.69}(C_4)$	s(37.15) p(62.85)
$BD^*(1)$	0.01009	$sp^{2.75}(C_3)$	s(26.66) p(73.34)
$C_3—C_8$		$sp^{2.41}(C_8)$	s(29.30) p(70.70)
$BD^*(1)$	0.04249	$sp^{2.14}(C_4)$	s(31.81) p(68.19)
$C_4—C_5$		$sp^{2.77}(C_5)$	s(26.49) p(73.51)
$BD^*(1)$	0.01229	$sp^{2.23}(C_4)$	s(30.98) p(69.02)
$C_4—O_7$		$sp^{1.33}(O_7)$	s(42.83) p(57.17)
$BD^*(1)$	0.02336	$sp^{2.72}(C_5)$	s(26.89) p(73.11)
$C_5—C_6$		$sp^{2.87}(C_6)$	s(25.85) p(74.15)
$BD^*(1)$	0.02540	$sp^{2.49}(C_6)$	s(28.62) p(71.38)
$C_6—C_9$		$sp^{2.11}(C_9)$	s(32.13) p(67.87)
$BD^*(1)$	0.02106	$sp^{1.90}(C_9)$	s(34.54) p(65.46)
$C_9—C_{10}$		$sp^{1.78}(C_{10})$	s(35.91) p(64.09)
$BD^*(1)$	0.02327	$sp^{2.00}(C_9)$	s(33.33) p(66.67)
$C_9—C_{14}$		$sp^{1.80}(C_{14})$	s(35.66) p(64.34)
$BD^*(1)$	0.01238	$sp^{1.83}(C_{10})$	s(35.35) p(64.65)
$C_{10}—C_{11}$		$sp^{1.81}(C_{11})$	s(35.56) p(64.44)
$BD^*(1)$	0.01348	$sp^{1.81}(C_{11})$	s(35.62) p(64.38)
$C_{11}—C_{12}$		$sp^{1.82}(C_{12})$	s(35.51) p(64.49)
$BD^*(1)$	0.01351	$sp^{1.81}(C_{12})$	s(35.55) p(64.45)
$C_{12}—C_{13}$		$sp^{1.82}(C_{13})$	s(35.47) p(64.53)
$BD^*(1)$	0.01284	$sp^{1.80}(C_{13})$	s(35.73) p(64.27)
$C_{13}—C_{14}$		$sp^{1.85}(C_{14})$	s(35.13) p(64.87)
$BD^*(1)$	0.02079	$sp^{1.90}(C_{15})$	s(34.44) p(65.56)
$C_{15}—C_{16}$		$sp^{1.79}(C_{16})$	s(35.88) p(64.12)
$BD^*(1)$	0.02516	$sp^{1.98}(C_{15})$	s(33.55) p(66.45)
$C_{15}—C_{20}$		$sp^{1.87}(C_{20})$	s(34.81) p(65.19)
$BD^*(1)$	0.01252	$sp^{1.84}(C_{16})$	s(35.23) p(64.77)
$C_{16}—C_{17}$		$sp^{1.81}(C_{17})$	s(35.55) p(64.45)
$BD^*(1)$	0.01329	$sp^{1.81}(C_{17})$	s(35.55) p(64.45)
$C_{17}—C_{18}$		$sp^{1.81}(C_{18})$	s(35.55) p(64.45)
$BD^*(1)$	0.01302	$sp^{1.82}(C_{18})$	s(35.47) p(64.53)
$C_{18}—C_{19}$		$sp^{1.83}(C_{19})$	s(35.38) p(64.62)
$BD^*(1)$	0.01646	$sp^{1.80}(C_{19})$	s(35.78) p(64.22)
$C_{19}—C_{20}$		$sp^{1.85}(C_{20})$	s(35.04) p(64.96)

10 NLO Properties

Polarizabilities and hyperpolarizabilities characterize the response of a system in an applied electric field. They determine not only the strength of molecular interactions as well as the cross-sections of different scattering and collision processes, but also the non-linear optical properties (NLO) of the system[33]. The second-order polarizability or first hyperpolarizabilityβ, dipole moment μ and polarizabilityα are calculated using B3LYP/6-311++G(d,p) basis set on the basis of the finite-field approach.

In the presence of an external electric field (E), the energy of the system is a function of the electric field. First hyperpolarizability is a third-rank tensor that can be described by a 3×3×3 matrix. The 27 components of the 3D matrix can be reduced to 10 components because of the Kleinman symmetry[34]. The components of β are defined as the coefficients in the Taylor series expansion of energy in an external electric field.

When an external electric field is weak and homogeneous, Taylor series expansion becomes:

$$E = E^0 - \frac{\mu_i F_i}{1!} - \frac{\alpha_{ij} F_i F_j}{2!} - \frac{\beta_{ijk} F_i F_j F_k}{3!} - \frac{\gamma_{ijkl} F_i F_j F_k F_l}{4!}$$

where E is the energy of the unperturbed molecules, F_i is the field at origin and μ_i, α_{ij}, β_{ijk} andγ_{ijkl} are the components of dipole moment, polarizability, first hyperpolarizabilities and the second hyperpolarize-abilities, respectively. The complete equations for calculating the magnitude of total static dipole moment μ, the mean polarizability α_0, the anisotropy of the polarizability $\Delta\alpha$ and the mean first polarizability β_{tot} using x, y and z components from Gaussian 09 output is as follows:

Dipole moment, $\mu = (\mu_x^2 + \mu_y^2 + \mu_z^2)^{1/2}$

Mean polarisability $\alpha_o = \dfrac{\alpha_{xx} + \alpha_{yy} + \alpha_{zz}}{3}$

Anisotropic polarisability

$$\Delta\alpha = 2^{-1/2}[(\alpha_{xx} - \alpha_{yy})^2 + (\alpha_{yy} - \alpha_{zz})^2 + (\alpha_{zz} - \alpha_{xx})^2 + 6\alpha_{xz}^2]^{1/2}$$

first-order polarisability $\beta_{tot} = (\beta_x^2 + \beta_y^2 + \beta_z^2)^{1/2}$ and

$$\beta_x = \beta_{xxx} + \beta_{yyy} + \beta_{zzz}$$
$$\beta_y = \beta_{yyy} + \beta_{xxy} + \beta_{yzz}$$
$$\beta_z = \beta_{zzz} + \beta_{xxz} + \beta_{yyz}$$

Table 10 — Electric dipole moment μ (Debye), mean polarizability α_o (10^{-22} esu), anisotropy polarizability $\Delta\alpha$ (10^{-25} esu) and first hyperpolarizability β_{tot} (10^{-31} esu) for MDPO

Parameters	Values	Parameters	Values
μ_x	0.3097	β_{xxx}	−5.8989
μ_y	−3.7455	β_{yyy}	−75.5792
μ_z	−0.9297	β_{zzz}	0.3078
μ	3.8715	β_{xyy}	11.4864
α_{xx}	−110.6647	β_{xxy}	−36.6550
α_{xy}	−0.5493	β_{xxz}	−19.4291
α_{xz}	−2.0401	β_{xzz}	−6.0989
α_{yy}	−139.3812	β_{yzz}	2.8540
α_{yz}	−1.5112	β_{yyz}	11.7813
α_{zz}	−113.4516	β_{xyz}	−2.5770
α_o	−121.16583	β_{tot}	109.6273
$\Delta\alpha$	27.6560		

The polarizabilities and hyperpolarizability are reported in atomic units (au). The hyperpolarizability β, dipole moment μ and polarizability α of MDPO are presented in Table 10. The calculated value of dipole moment was found to be 3.8715 Debye. The highest value of dipole moment is observed for component μ_x. In this direction, this value is equal to 0.3097 Debye. The calculated polarizability and anisotropy of the polarizability of MDPO are -121.16583×10^{-22} esu and 27.6560×10^{-25}esu, respectively. The magnitude of the molecular hyperpolarizability β is found to be 109.6273×10^{-31}esu and is one of the important key factors in a NLO system[35]. The calculated value of β suggests the usefulness of the piperidine as catalyst in chemical reactions to enhance NLO character. The dipole moment and first hyperpolarizability of title molecule can be compared with those of urea (μ and β of urea are 1.525686Debye and 0.780324×10^{-30}esu obtained by B3LYP/6-311++G(d,p) method). Since urea is one of the prototypicalmolecules used in the study of the NLO properties of molecular systems, it was used frequently as a threshold value for comparative purpose.

11 Conclusions

A complete vibrational analysis has been carried out for MDPO using FT-IR and Raman spectroscopy. Assignments of the vibrational spectra have been facilitated by DFT calculation. A good correlation was found between the computed and experimental wavenumbers.The molecular structural parameters like bond length, bond angle, torsional angle and dihedral angle have been determined from *ab-initio* and DFT calculations using 6-311++G(d,p) basis set. Mulliken charges of MDPO at different levels were calculated and the results discussed. HOMO, LUMO energies and HOMO-LUMO energy gap are calculated as 4.9427 eV. The delocalization pattern of charge and electron densities of MDPO molecule have been explained by performing molecular orbital simulations at HF method with 6-311 ++G basis set. The stabilization of the structure has been identified by second order perturbation energy calculations. The calculation of first hyperpolarizability gives MDPOs utility as catalyst to increase NLO properties. The UV analysis gives the electronic spectrum of MDPO that has revealed the allowed and forbidden transitions with solvent effects.

Acknowledgement

The authors sincerely acknowledge the support from the Department of Physics, PSG College of Arts & Sciences, Coimbatore, Tamilnadu, India to synthesise and take FT-IR and UV testing. They also thank to SAIF, Indian Institute of Technology, Chennai, Tamilnadu, India to take the FT-Raman test of the sample and the faculties of Department of Physics, K S Rangasamy College of Technology, Tiruchengode, Namakkal, Tamilnadu, India for the encouragement they rendered throughout this work.

References

1 Rubiralta M, Giralt E & Diel A, *Piperidine Structure, Preparation and Synthetic Applications of Piperidine and its Derivatives* (Elsevier, Amsterdam) 1991.
2 Lijinsky W & Taylor H W, *Int J Cancer*, 16 (1975) 318.
3 Prostakov N S &Gaivoronskaya L A, *Russ Chem Rev*, 47 (1978) 447.
4 Jerom B R & Spencer K H, *Eur Pat Appl*, EP 277794 (1988)
5 Schneider M J, in S W Pelletier (Ed.), *Alkaloids: Chemical and Biological Perspectives*, Wiley, New York, 10 (1996) 155.
6 El-Subbagh H I, Abu-Zaid S M, Mahran M A, Badria F A & Alobaid A M, *J Med Chem*, 43 (2000) 2915.
7 Scott L J & Spencer C M, *Drugs*, 59(3) (2000) 521.
8 Erdogdu Y &Gulluoglu M T, *Spectrochim Acta A*, 74 (2009) 162.
9 Frisch M J *et al*. *Gaussian 09*, Revision C.01, (Gaussian, Inc., Wallingford CT), 2010.
10 Becke A D, *J Chem Phys*, 98 (1993) 5648.
11 Rauhut G &Pulay P, *J PhysChem*, 99 (1995) 3093.
12 Pulay P, Fogarasi G, Pongor G, Boggs J E & Vargha A, *J Am Chem Soc*, 105 (1983) 7037.
13 Fogarasi G, Zhou X, Taylor P W & Pulay P, *J Am Chem Soc*, 114 (1992) 8191.
14 Keresztury G, Holly S, Vargha J, BasenyeiG, Wang A Y & Durig J R, *Spectrochim Acta A*, 49 (1993) 2007.
15 Keresztury G, in: Chalmers J M, Griffith P R (Eds), *Raman spectroscopy: Theory in Handbook of vibrational spectroscopy*, John Wiley & sons Ltd., 2002.
16 Subashchandrabose, Saleema H, Erdogdu Y, Rajarajan G & Thanikachalam V, *SpectrochimicaActa Part A*, 82 (2011) 260.
17 Gulluoglu M T, Erdogdu Y &Yurdakul S, *J MolStruct*, 834 (2007) 540.
18 Erdogdu Y, Gulluoglu M T & Yurdakul S, *J MolStruct*, 889 (2008) 361.
19 Erdogdu Y & Gulluoglu M T, *Spectrochim Acta PartA*, 74 (2009) 162.
20 Vedal D, Ellestad O & Klaboe P, *Spectrochim Acta A*, 32(1976) 877.
21 Tzeng W B, Narayanan K, Lin J L & Tung C C, *Spectrochim Acta A*, 55 (1998)153.
22 Roeges N P G, *A Guide to the Complete Interpretation of Infrared Spectra of Organic Structures* (Wiley, New York), 1994.
23 Sajan D, Binoy J, Pradeep B, Krishnan K V, Kartha V B, Joe I H & Jayakumar V S, *Spectrochim. Acta A,* 60 (2004) 173.
24 Druz˙ bicki K, Mikuli E & Ossowska-Chru´sciel M D, *Vib Spectrosc*, 52 (2010) 54.
25 Gulluoglu M T, Erdogdu Y & Yurdakul S, *J MolStruct*, 834 (2007) 540.
26 Sundaraganesan N, Illakiamani S, Meganathan C & Joshua B D, *Spectrochim Acta* A, 67 (2007) 214–224.
27 Erdogdu Y & Gulluoglu M T, *Spectrochim Acta A*, 74 (2009) 162.
28 Fukui K, Yonezawa T & Shingu H, *J Chem Phys*, 20 (1952) 722.
29 Reed A E & Weinhold F, *J Chem Phys*, 83 (1985) 1736.
30 Reed A E, Weinstock R B & Weinhold F, *J Chem Phys*, 83 (1985) 735.
31 Reed A E & Weinhold F, *J Chem Phys*, 78 (1983) 4066.
32 Foster J P & Wienhold F, *J Am Chem Soc*, 102 (1980) 7211.
33 Sun Y, Chen X, Sun L, Guo X & Lu W, *Chem Phys Lett*, 381 (2003) 397.
34 Kleinman D A, *Phys Rev*, 126 (1962) 1977.
35 Shanmugam G, Thirupugalmani K, Kannan V & Brahadeeswaran S, *Spectrochimica Acta Part A: Molecular and Biomolecular Spectroscopy*, 106 (2013) 175.
36 Anbarasu P, Arivazhagan M & Balachandran V, *Indian J Pure & Appl Phys*, 50 (2012) 91.
37 Zhou Z R, Hong L X & Zhou Z X, *Indian J Pure & Appl Phys*, 50 (2012) 719.
38 Balachandran V, Karthick T, Perumal S & Nataraj A, *Indian J Pure & Appl Phys*, 51(2013)178.
39 Balasubramanian M & Padma N, *Tetrahedron*, 19 (1963) 2135.
40 KuppusamySelvaraj, Manjula Narasimhan & Jaganathan Mallika, *Transition Metal Chemistry*, 26 (2001) 224.